

Activity-Based Photoacoustic Probes for Detection of Disease Biomarkers beyond Oncology

Michael C. Lee, Kayla Landers, and Jefferson Chan*



Cite This: *ACS Bio Med Chem Au* 2023, 3, 223–232



Read Online

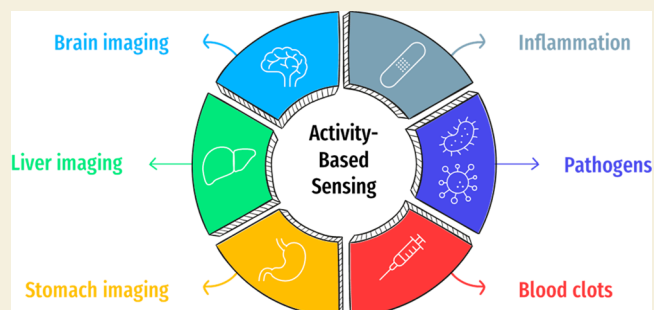
ACCESS |

Metrics & More

Article Recommendations

ABSTRACT: The earliest activity-based photoacoustic (PA) probes were developed as diagnostic agents for cancer. Since this seminal work over a decade ago that specifically targeted matrix metalloproteinase-2, PA instrumentation, dye platforms, and probe designs have advanced considerably, allowing for the detection of an impressive list of cancer types. However, beyond imaging for oncology purposes, the ability to selectively visualize a given disease biomarker, which can range from aberrant enzymatic activity to the overproduction of reactive small molecules, is also being exploited to study a myriad of noncancerous disease states. In this review, we have assembled a collection of recent papers to highlight the design principles that enable activity-based sensing via PA imaging with respect to biomarker identification and strategies to trigger probe activation under specific conditions.

KEYWORDS: biomedical imaging, human diseases, activity-based sensing, activatable probes, photoacoustic, biomarkers, *in vivo*, molecular imaging, optoacoustic, preclinical



1. INTRODUCTION

Photoacoustic (PA) imaging is a state-of-the-art imaging technique that allows for detailed *in vivo* imaging. This modality grants access to previously elusive and inaccessible molecular images with robust depth, precision, and accuracy, revolutionizing the field of molecular imaging. By exploiting the PA effect where optical excitation of a chromophore generates pressure waves which are detected as sound, PA imaging has successfully overcome the limitations of poor resolution in deep tissue that is associated with light-based methods. Initial work in the PA field focused on label-free imaging by employing endogenous light absorbing chromophores such as hemoglobin and melanin to generate contrast.^{1,2} However, label-free imaging restricts the broad potential of PA imaging due to the inability to detect essential nonlight absorbing biomarkers.

Seminal work by Gambhir and co-workers demonstrated the potential of this modality for cancer diagnostics and monitoring by targeting matrix metalloproteinase-2 (MMP-2) activity utilizing a design that consisted of two PA-active molecules appended together by a peptide substrate.³ MMP-2-mediated cleavage of the probe at the tumor site separates the components, leading to a change in the PA ratio. Since this work over 10 years ago, improvements with respect to instrumentation, dye platforms, and probe designs have been nothing short of revolutionary, lead to major advances in PA cancer imaging. In particular, activity-based sensing (ABS)

designs have greatly expanded upon what was possible relative to traditional binding-based sensors (Scheme 1).^{4–7} Because ABS exploits the chemical reactivity of the analyte, they can be readily tuned to maximize interaction with the biomarker of interest. Furthermore, properties such as the kinetics of the probes can be adjusted to accelerate or attenuate reactivity to target transient or longer lasting (or abundant) molecular events, respectively.

In the present review, we highlight ABS probes for PA imaging that focus on noncancer applications. This will include work that target biomarkers found in organ systems such as the brain (section 2), liver (section 3), and stomach (section 4). Additionally, we discuss PA probes that enable the detection of inflammatory markers (section 5), as well as pathogens such as bacteria and viruses that cause infections (section 6). Finally, we will focus on examples that enable the visualization of biomarkers linked to a variety of blood clotting conditions (section 7).

Received: February 3, 2023

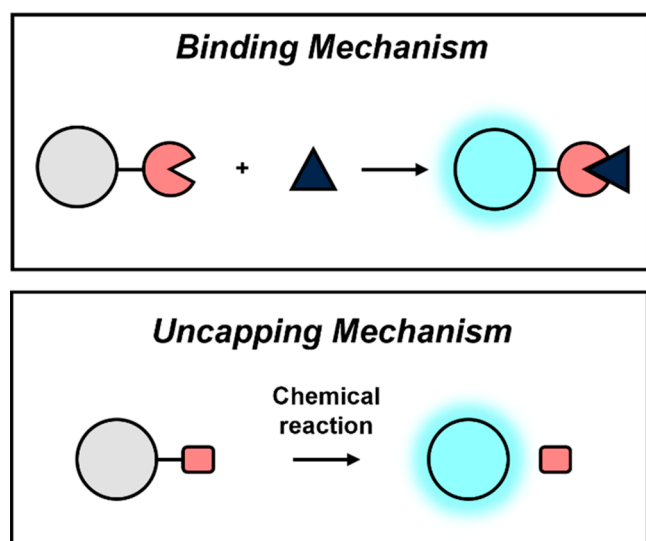
Revised: February 27, 2023

Accepted: February 28, 2023

Published: March 10, 2023



Scheme 1. Schematic Demonstrating Different Probe Design Strategies^a



^aThe binding mechanism (top) involves signal enhancement upon interaction between the probe and target. On the other hand, probe activation *via* an uncapping mechanism (bottom) involves cleavage and separation of the trigger from the PA reporter. Responsive element shown in pink.

2. BRAIN IMAGING

The brain is one of the most complex organs in the human body, and work is still ongoing to demystify biological processes within this organ.⁸ Leveraging molecular imaging to study the mechanistic underpinnings of pathophysiological states can expedite the discovery of new treatment options. However, imaging of the brain is not trivial when employing molecular probes owing to low permeability through the blood–brain barrier (BBB), as well as a reliance on invasive procedures (*e.g.*, generation of intracranial windows) to facilitate imaging studies. In this regard, advances in PA imaging and development of new BBB compatible imaging agents have allowed for noninvasive imaging of the brain to detect various biomarkers (*e.g.*, calcium, lithium, ROS) in a manner that was previously not possible.⁹ We highlight recent work below in this area.

2.1. Emerging Alzheimer's Disease Biomarkers

Alzheimer's disease (AD) is a neurological disorder that impacts over 6 million individuals in the United States alone.¹⁰ It is characterized by the accumulation of tau proteins and beta amyloid plaques which have been hypothesized to be key culprits in causing mental impairment and dementia.¹¹ Besides these well-recognized hallmarks, AD has also been linked to an increase of reactive oxygen species (ROS) production (*e.g.*, hydrogen peroxide (H_2O_2)), as well as the accumulation of redox-active metals such as Cu^{2+} .

To detect H_2O_2 in AD brains, it is critical to employ a PA reporter capable of producing a strong signal upon irradiation. Toward this end, Chan and co-workers remodeled the canonical hemicyanine dye (HD) by substituting the endocyclic oxygen with a sulfur atom, which red shifts the absorbance of the dye by ~ 50 nm and concomitantly decreases the fluorescence quantum yield by 85% (to favor ultrasound (US) production).¹² Moreover, the authors installed an *ortho*-chloro group to acidify the phenolic position, which ensures

the dye is deprotonated at physiological pH to exhibit a larger extinction coefficient relative to the parent molecule. Capping of the resulting dye (named PA-HD) with an aryl boronate trigger led to the development of PA-HD- H_2O_2 . An ensuing reaction with H_2O_2 converts the aryl boronate into a phenol, which spontaneously collapses to release PA-HD *via* quinone-methide elimination chemistry (Figure 1a). In their study, PA-

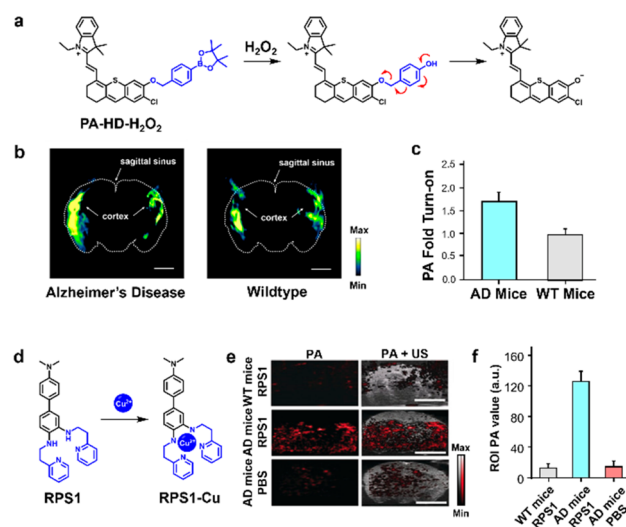


Figure 1. (a) Schematic of the reaction between PA-HD- H_2O_2 and H_2O_2 to afford PA-HD. (b) Spectrally unmixed PA images of AD and WT brain. Sagittal sinus and cortex indicated by arrows. (c) Quantified data from (b). (d) Schematic of reaction between RPS1 and $\text{Cu}(\text{II})$. (e) PA (left) and PA and ultrasound (right) images of WT mice and AD mice treated with RPS1 (top and middle rows, respectively), and AD mice administered a PBS vehicle control. (f) Quantified data from (e). Adapted with permission from refs 12 and 14. Copyright 2021 and 2019 Wiley.

HD- H_2O_2 was successfully employed to assess oxidative stress (*via* H_2O_2 detection) in AD mice (Figure 1b). Relative to age-matched wild-type (WT) animals where the change in the PA signal over time was only 1.02, the corresponding increase was 1.79 in the AD model (Figure 1c). To verify that this was due to probe activation and not dye accumulation, ratiometric analysis was employed. The observed ratiometric PA signal change was 1.23 and 0.85 in AD mice and WT mice, respectively.

A potential cause of elevated oxidative stress in the brain of AD mice may be due to Cu dysregulation. Specifically, it has been hypothesized that Cu^{2+} reacts with H_2O_2 *via* Fenton-like chemistry to yield free radicals which is linked to the assembly of amyloid beta fibrils characteristic of AD.¹³ Since crossing the BBB is a challenge for large contrast agents and activatable imaging probes, Sheng, Zhang, and co-workers designed RPS1, a Cu^{2+} -responsive PA probe that boasts a relatively low molecular weight of 438 Da.¹⁴ RPS1 features an aniline-based chelator, which upon binding to Cu^{2+} , leverages the redox chemistry of this metal ion to form an aniliny radical cation species that exhibits a red-shifted λ_{PA} in the NIR region (Figure 1d). Selectivity assays against a panel of divalent metal ions demonstrate excellent selectivity for Cu^{2+} . To examine its ability to pass the BBB for *in vivo* applications, the authors conducted an experiment to show its permeability through a transwell cell monolayer model that mimics features of the BBB. Additionally, these findings were confirmed in a murine

model of AD. Subsequent PA imaging resulted in a 9.57-fold increase in the signal intensity relative to non-AD control mice and an 8.5-fold increase when compared to PBS vehicle-treated AD mice (Figure 1e,f). To further corroborate these results, the authors confirmed plaque deposition and shrunken cell nuclei in AD brain slices, indicative of neurodegeneration.

2.2. Calcium Detection

Calcium ions (Ca^{2+}) plays a key role in cellular messaging, contractility of muscles, immunity, and neuron signaling.¹⁵ However, many chemical tools to study Ca^{2+} *via* molecular imaging are not suited for deep brain imaging and often requires generation of invasive intracranial windows.¹⁶ As such, PA probes for this metal ion have the potential to overcome this long-standing challenging by exploiting an ultrasound readout. To this end, Westmeyer and co-workers developed CaSPA, a cell-permeable and calcium-selective PA sensor.¹⁷ The design principle behind CaSPA relies on appending BAPTA (a common Ca^{2+} chelator) onto a semicyanine chromophore (Figure 2a). Upon interaction between Ca^{2+}

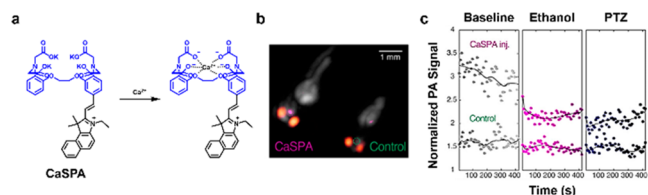


Figure 2. (a) Chemical structure of CaSPA and CaSPA– Ca^{2+} complex. (b) Representative PA images of zebrafish to visualize Ca^{2+} fluxes in the brain. Purple regions indicate signal from CaSPA, and the orange regions indicate the melanin-containing eyes. (c) Quantified signal before (top curve) and after (bottom curve) treatment with ethanol or PTZ. Adapted from ref 17. Copyright 2018 American Chemical Society.

by the BAPTA ligand, a photoinduced charge transfer (PCT) event leads to a hypsochromic shift of the probe absorbance profile which has the effect of yielding a turn-off response. CaSPA was applied to an *in vivo* model to visualize Ca^{2+} fluxes. Specifically, CaSPA-treated and nontreated control zebra fish were embedded in agar and PA imaging was employed to visualize this metal ion (Figure 2b). Ethanol and pentylene-tetrazole (PTZ), two established neuro stimulants that trigger the release of Ca^{2+} was employed as stimulants. Under both conditions, the authors observed a notable attenuation of the PA signal indicating a binding event had taken place between Ca^{2+} and CaSPA (Figure 2c).

2.3. Stem Cell Tracking

Stem cell therapies are being explored to treat a myriad of diseases. However, tracking the fate of stem cells once introduced *in vivo* has been a challenge. To further study the downstream effects of stem cells, Jokerst and co-workers utilized PA imaging to visualize human mesenchymal stem cells (hMSCs) *via* labeling with Prussian blue nanoparticles (PBNPs) (Figure 3a).¹⁸ PBNPs were employed due to its biocompatibility, NIR absorption, stability, and strong PA signal upon irradiation. However, PBNPs have a negative zeta potential, resulting in poor cellular uptake due to charge repulsion with cell membranes. To circumvent this, PBNPs developed in this study were complexed with poly-L-lysine to yield nanocomplexes exhibiting a positive zeta potential. To ensure PBNPs did not alter the stemness properties of hMSCs,

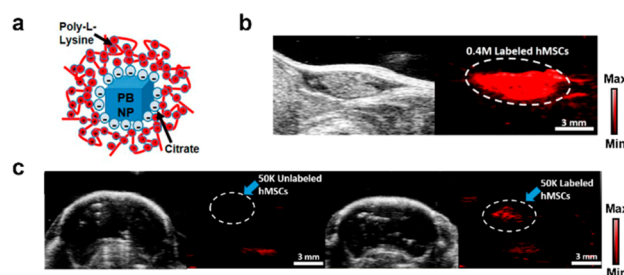


Figure 3. (a) Structure of encapsulated nanoparticle. (b) Representative US (left) and PA (right) image of labeled hMSCs. (c) Representative US and PA images of unlabeled and labeled hMSCs in mouse brain imaging. Adapted from ref 18. Copyright 2017 American Chemical Society.

flow cytometry was conducted to confirm the presence of three stem cell surface markers: CD73, CD90, and CD105. Further characterization revealed a detection limit of 100 cells/ μL and retention of the contrast agent for at least 2 weeks. Labeled and unlabeled hMSCs were injected subcutaneously in mice and imaged (Figure 3b). The authors were able to observe a sustained PA signal when 50,000 cells were introduced. Due to these promising results, hMSCs were then introduced to the brain *via* intraparenchymal injections to mimic stem cell transplantations in ischemic brain regions characteristic in stroke patients. Labeled hMSCs exhibited a 9.8-fold increase in PA signal increase in the brain, allowing for its detection *in vivo* (Figure 3c).

3. LIVER IMAGING

As mentioned above, the liver plays a crucial role in human physiology due to its function in detoxifying xenobiotics. Because of the wide range of toxins that the liver encounters, it is susceptible to damage from drugs, ingested foods, and harmful chemicals from the environment. Of note, while inflammation is a common property of liver injury, we will cover this feature in the following section. Beyond the inflammatory response, a wide range of biomarkers ranging from the production of ROS to increased activity of certain liver enzymes has also been associated with liver damage. By taking advantage of these changes, the diversity of activatable probes suitable for molecular imaging of the liver has greatly expanded.

3.1. Elevated Cu in Wilson's Disease

Wilson's disease (WD) is a genetic disorder caused by a mutation in the gene encoding ATP7B, a membrane-associated Cu-transporting protein that predominantly impacts the brain and liver. The resulting accumulation of Cu in these organs leads to severe tissue damage which can be fatal if not treated. The levels of Cu in a WD patient are typically assessed through blood tests and invasive liver biopsies.¹⁹ Chan and co-workers recently introduced a noninvasive PA imaging alternative based on the application of PACu-1, the first acoustogenic probe for Cu^+ visualization.²⁰ PACu-1 features a Cu^+ -responsive TPA trigger appended to an aza-BODIPY dye through a cleavable ether linkage (Figure 4a). Release of the free dye after an oxidative cleavage event results in a red shift of the λ_{abs} by ~ 90 nm which is exploited for ratiometric calibration. Of note, the +1-oxidation state was targeted as opposed to Cu^{2+} because it is the predominate form in the liver owing to the highly reducing environment rich in GSH (10 mM). Upon successfully demonstrating PACu-1 is safe to use in living

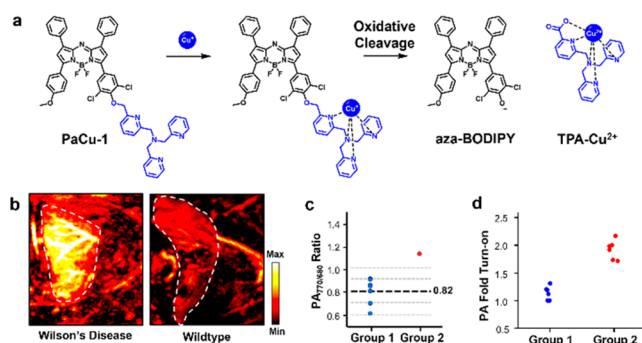


Figure 4. (a) Structure of PaCu-1 and its mechanism of activation after undergoing a redox reaction with Cu^+ . (b) Representative PA images of WD mice and wild-type mice and (c) its ratiometric signal to identify WD from a cohort of animals in a blind study. (d) PA fold turn-on of mice in a second blind study to stratify a group of WD and wildtype mice *via* the extent of signal enhancement. Adapted with permission from ref 20. Copyright 2021 National Academy of Sciences.

subjects, it was employed to measure hepatic Cu *via* biopsy-free assessment (BFA) in a murine model of WD. To remove potential experimental bias, the authors designed and executed two blind studies. First, they successfully identified a single WD mouse out of a group consisting of a total of eight mice that were randomly selected from a larger pool of animals (Figure 4b,c). Second, a group of 12 animals consisting of six WD and six wild-type mice were randomized, and their identities were concealed from the experimenter. Using PaCu-1 *via* PA imaging, the authors were able to correctly stratify each of the 12 animals with a success rate of 100% (Figure 4d). Overall, this work sets the stage to use other biocompatible PA imaging agents to complement invasive biopsies for biomarker detection.

3.2. Liver Injury Monitoring

As mentioned above, the liver plays a crucial role in human physiology due to its function in detoxifying xenobiotics. Because of the wide range of toxins that the liver encounters, it is susceptible to damage from drugs, ingested foods, and harmful chemicals from the environment. A wide range of biomarkers ranging from the production of ROS to increased activity of certain liver enzymes has been associated with liver damage. By taking advantage of these changes, the diversity of activatable probes suitable for molecular imaging of the liver has greatly expanded.^{21–29}

ROS are known to nonspecifically interact with a multitude of molecules and biomolecules. Additionally, the superoxide anion radical ($\text{O}_2^{\bullet-}$) has been found at higher concentrations in damaged livers. To take advantage of the chemical reactivity of this ROS for molecular imaging, Ren, Yuan, and co-workers developed AP, an aza-BODIPY-based ratiometric PA probe for liver imaging (Figure 5a).³⁰ To enhance solubility and introduce a targeting group to the liver, β -galactose was appended to the dye scaffold through a water solubilizing PEG linkage. Furthermore, the dye was capped with a trifluoromethanesulfonate trigger due to its electron-deficient properties as well as its selectivity for $\text{O}_2^{\bullet-}$. Upon reaction with $\text{O}_2^{\bullet-}$, the trigger is removed to release the latent dye. Of note, this uncapping process also induces a bathochromic shift when compared to the capped probe. To test their lead molecule in cells, the authors confirmed galactose-mediated uptake, as well as probe turnover in an LPS-induced liver injury model in L02

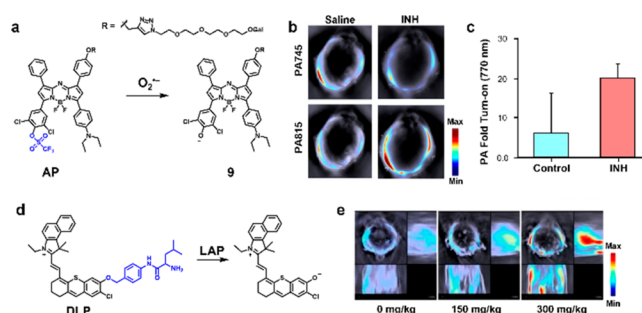


Figure 5. (a) Structure and turnover product of AP. (b) Representative cross-sectional PA images of an INH-induced liver injury model and saline control acquired at $t = 40$ min. (c) Quantified PA fold turn-on. (d) Structure and turnover product of DLP. (e) Representative cross-sectional and lateral PA images of an acetaminophen-induced liver injury model. Adapted from refs 30 and 31. Copyright 2022 and 2019 American Chemical Society.

cells. To determine its efficacy for *in vivo* imaging, the probe was introduced to an isoniazid (INH)-induced liver injury model (Figure 5b). A ratiometric turn-on of 1.5-fold at $\text{PA}_{815}/\text{PA}_{745}$ was observed, while the ratiometric signal for the saline control was less than 1 (Figure 5c). Finally, pretreatment with *N*-acetylcysteine (an ROS scavenger) prior to INH injection decreased the ratiometric turn-on, indicating its antioxidant properties.

Apart from ROS generation, liver injury also leads to various downstream effects, including the overexpression of enzymes such as leucine aminopeptidases (LAP). Zeng, Wu, and co-workers developed a probe (DLP) based on the hemicyanine dye platform to detect this enzymatic activity (Figure 5d).³¹ A leucyl group was appended on to the chromophore *via* a self-immolative 4-aminobenzylalcohol linker to mimic an *N*-terminal leucine. Upon cleavage by LAP, the linker undergoes a quinone methide elimination to release the free dye. The probe was then tested against a panel of metal ions, ROS, biomolecules, and enzymes to show negligible response. Further, the probe was tested in HepG2 human liver cells for LAP activity. Upon pretreatment with bestatin, a LAP inhibitor, the PA signal significantly decreased which supports the mode of action of their probe. To generate a liver injury model, mice were intraperitoneally injected with acetaminophen. Subsequent injection of the probe enabled PA imaging of liver injury *via* LAP upregulation with a signal that peaked 30 min post dye administration. Additionally, the authors were able to show a dose-dependent signal increase when liver injury was induced with higher dosages of acetaminophen (Figure 5e). Finally, *ex vivo* imaging corroborated the stronger PA signal within the liver compared to other major organs and H&E staining validated macrophage infiltration.

4. STOMACH IMAGING

Dysregulation of stomach pH is indicative of many pathologies. For instance, gastric ulcers cause a change of the stomach pH (3.4) compared to healthy subjects (2.9). Similarly, esophageal ulcers and duodenal ulcers also alters the pH (1.9 and 2.1, respectively) in the stomach. To enable PA imaging of stomach pH, Sarma, Sessler, Liu, and co-workers developed a panel of expanded porphyrins.³² Their lead porphyrin, octaphyrin, was encapsulated in DSPE-PEG₂₀₀₀ to yield OctaNPs (Figure 6a). Under acidic redox conditions, OctaNPs undergo a CPET (concerted proton electron transfer) process. Since gastric acid

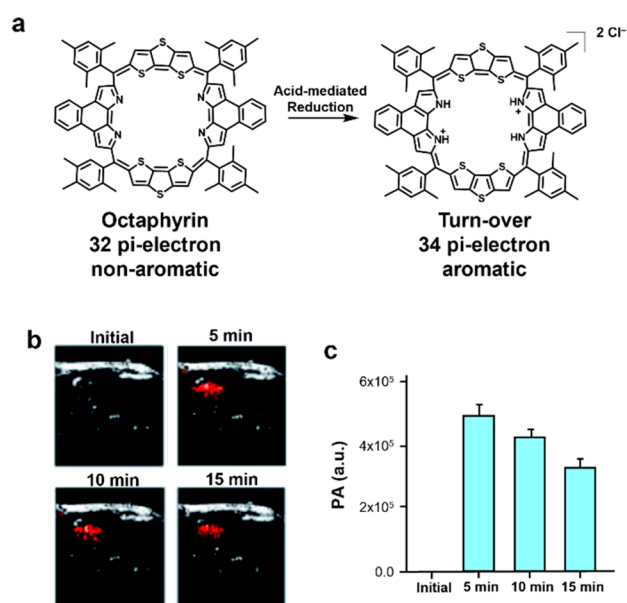


Figure 6. (a) Chemical structure of octaphyrin and its turnover product. (b) Representative PA images of the stomach area of mice before and after injection with octaphyrin. (c) Quantified PA signal. Adapted with permission under CCBY 3.0 license from ref 32. Copyright 2021 Royal Society of Chemistry.

is composed of redox active hydrochloric acid, octaphyrin is reduced from the 32 π -electron nonaromatic state to the 34 π -electron aromatic state, leading to an increased in absorbance at 1200 nm. To test OctaNP *in vivo*, mice were subjected to intragastric injection, resulting in an immediate increase in PA signal when excited, indicative of a low stomach pH (Figure 6b,c). Additionally, to visualize dynamic changes, mice were pretreated with sodium bicarbonate to neutralize the acidic stomach environment. Upon injection of OctaNP, no PA signal enhancement was observed. However, over a period of 15 min, secretion of gastric acid restores the pH of the stomach, resulting in a gradual PA signal enhancement.

5. INFLAMMATION IMAGING

Inflammation is a central process to the body's ability to illicit an immune response when challenged with a pathogen. However, a chronic inflammatory state is also known to exacerbate various human disease states. What is known in this regard is that inflammation is a complex process involving biomarkers ranging from enzymatic systems to small molecule mediators. Owing to its broad implications in health, significant efforts have been made to develop PA probes to detect inflammatory biomarkers.

5.1. MGL and FAAH Activity Sensing

Monoacylglycerol lipase (MGL) and fatty acid amide hydrolase (FAAH) are two important enzymes of the endocannabinoid system (ECS).³³ Both are responsible for producing arachidonic acid (AA), which is a molecule involved in inflammation and energy metabolism. The major difference between MGL and FAAH activity is highlighted by the linkages they hydrolytically cleave. Specifically, MGL processes ester bonds, while FAAH hydrolyzes amides; however, it is noteworthy that there is significant cross-reactivity when considering the substrate scope. For instance, FAAH can hydrolyze both of these linkages with nearly identical rate

constants. It is this undesirable cross-reactivity that has precluded the development of enzyme-selective tools to investigate these enzymes in the context of inflammation. To overcome this challenge, ABS-tuning was employed by Chan and co-workers to stabilize the ester bond (via orbital interactions) of a new MGL probe.³⁴ Likewise, the authors prepared a selective substrate for FAAH by linking a PA reporter to AA through an amide bond. The resulting probes, PA-HD-MGL and PA-HD-FAAH (Figure 7a,b), exhibit

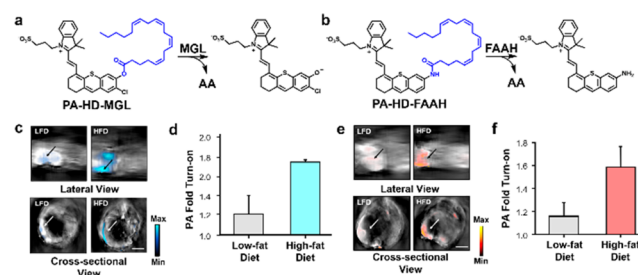


Figure 7. (a) Structure of PA-HD-MGL and (b) PA-HD-FAAH and their turnover products. (c) Representative lateral and cross-sectional PA images and (d) PA fold turn-on between low-fat diet (LFD) and high-fat diet (HFD) mice for PA-HD-MGL. (e) Representative lateral and cross-sectional PA images and (f) PA fold turn-on between LFD and HFD mice for PA-HD-FAAH. Adapted with permission from ref 34. Copyright 2022 Wiley.

excellent enzyme selectivity profiles and favorable PA imaging properties. *In cellulo* studies using LNCaP cells, which is a prostate cancer cell line known to express high levels of both enzymes, allowed the authors to confirm target engagement using small-molecule inhibitors. PA-HD-MGL and PA-HD-FAAH were then employed in a high-fat diet-induced obesity model. Cross-sectional and lateral view PA imaging of the gastrointestinal tract of obese animals revealed a 1.59-fold and 1.74-fold higher signal compared to the control group that was fed a low-fat diet using PA-HD-MGL (Figure 7c,d) or PA-HD-MGL (Figure 7e,f), respectively. These results implicate that upregulation of MGL and FAAH activity may be a driver of inflammation in obese animals.

5.2. Nitric Oxide Detection

Nitric oxide (NO) is an important gasotransmitter used by the body for signaling, homeostatic maintenance, and the modulation of the inflammatory response.³⁵ However, detecting NO within a living system is an immense challenge owing to its short biological half-life (second range) that results from its high reactivity with an abundance of nucleophilic species. Chan and co-workers addressed this by preparing a panel of five ABS probes featuring different known triggers.³⁶ They found the installation of an *N*-methylaniline trigger onto an aza-BODIPY dye, not only enabled rapid trapping of NO (via the active species N_2O_3) to yield a *N*-nitrosated product, but that this reaction was accompanied by a 91 nm blue shift (764 to 673 nm) (Figure 8a). Of note, molecules such as APNO-5 that can undergo distinct and dramatic changes in their spectral properties upon analyte detection are ideal for ratiometric imaging. To induce an inflammatory response *in vivo*, the authors treated mice with LPS (major component of Gram-negative bacteria cell walls) prior to the application of APNO-5 or a saline vehicle control. PA imaging was then performed at 770 and 680 nm to detect the probe and product, respectively (Figure 8c). The authors

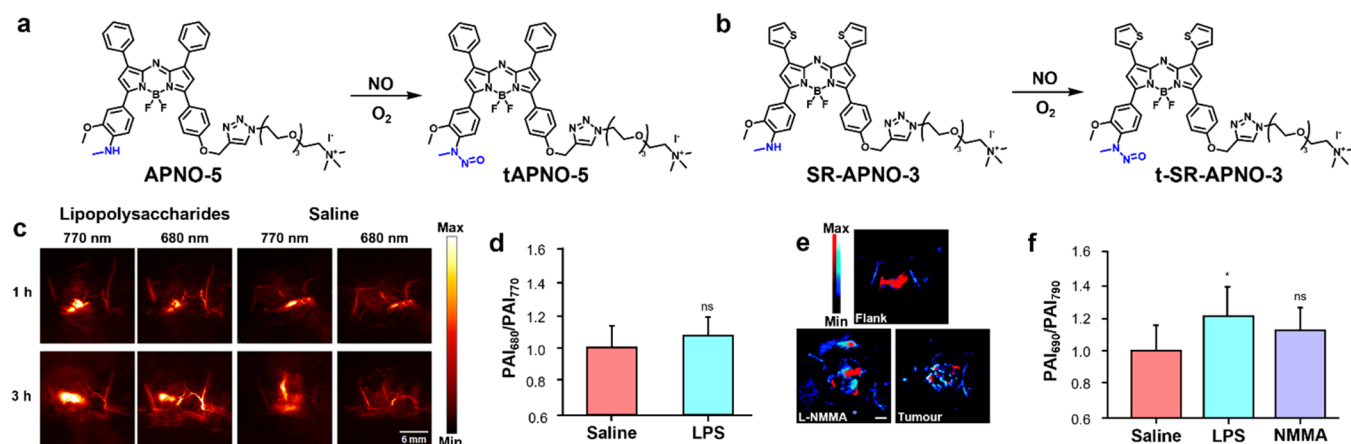


Figure 8. (a) Structure of APNO-5 and (b) SR-APNO-3. (c) Representative photoacoustic images of APNO-5 in a murine LPS-induced inflammation model and (d) ratiometric PA imaging (PAI_{680}/PAI_{770}) of NO in a LPS-induced inflammation model through intramuscular administration of APNO-5. Adapted from ref 36. Copyright 2018 American Chemical Society. (e) Representative image overlays corresponding to t-SR-APNO-3 (690 nm, blue) and SR-APNO-3 (790 nm, red) after 6 h subcutaneous or intratumoral administration and (f) ratiometric PA imaging (PAI_{690}/PAI_{790}) of NO in a LPS-induced inflammation model through intramuscular administration of SR-APNO-3. Adapted with permission under a CCBY 3.0 license from ref 37. Copyright 2020 Royal Society of Chemistry.

observed a change in the ratiometric signal (PAI_{680}/PAI_{770}) relative to a saline control over time, representing a 1.31-fold ratiometric turn-on (Figure 8d). Despite successfully detecting NO in this context, the authors subsequently prepared a congener (named SR-APNO-3) that was found to be 4.4-fold more sensitive than APNO-5 (Figure 8b).³⁷ This was accomplished by replacing both phenyl groups (on the top hemisphere of APNO-5) with thiophene units which increased the extinction coefficient by facilitating dye planarization through steric relaxation. Moreover, the authors noted a decreased quantum efficiency *via* the heavy-atom effect. Not only did these improvements enable detection of NO in the LPS-induced inflammation model described above, but the authors were also able for the first time to detect NO in tumors, which is present at levels orders of magnitude lower *via* PA imaging (Figure 8e,f).

5.3. Osteoarthritis Visualization

Degenerative joint disorders are also characterized by inflammation. Patients afflicted with these conditions experience cartilage degeneration which ultimately leads to osteoarthritis (OA). On a molecular level, glycosaminoglycans (GAGs) are an important component of cartilage that carries negative charges. Taking advantage of this property, Yu, Fan, and co-workers encapsulated water-soluble PA-active melanin nanoparticles (MNPs) with poly-L-lysine to develop PLL-MNPs that have a positive surface charge (+32.5 mV) (Figure 9a).³⁸ Due to charged interactions between GAGs and PLL-MNPs, healthy joints with intact cartilage will exhibit higher PA signal due to higher retention of the contrast agent. An *in vitro* experiment was performed where cartilage samples were incubated in PLL-MNPs or MNPs to demonstrate that the mechanism involves Coulombic interactions. Following washes with cold PBS, PA imaging revealed higher a signal intensity for PLL-MNP incubation (2580 au) when compared to MNP incubation (1425 au) after 24 h. Furthermore, PLL-MNPs were employed in an OA mouse model by surgically destabilizing the medial meniscus. OA mice exhibited a lower PA signal (1441 au) when compared to the sham-treated control mice (2113 au) (Figure 9b,c). Subsequently, H&E staining revealed higher inflammatory cell infiltration and

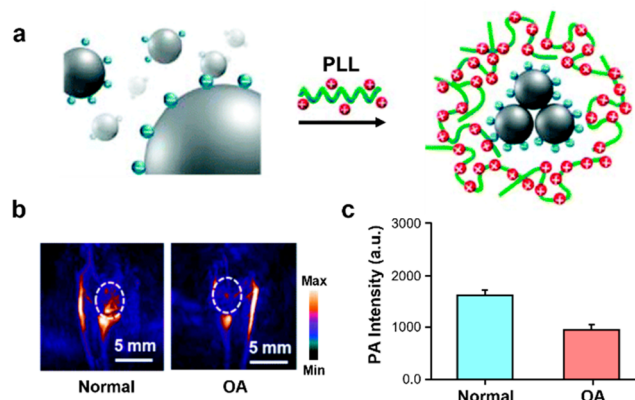


Figure 9. (a) Structure and assembly of PLL-MNPs. (b) Representative PA images of normal mice and osteoarthritis mice. (c) Quantified PA signal. Adapted with permission from ref 38. Copyright 2018 Royal Society of Chemistry.

Safranin-O staining corroborated decreased GAGs in the OA model when compared to sham mice.

6. PATHOGEN IMAGING

6.1. Bacteria Detection

Bacterial infections have increasingly become prevalent due to the rise of multi-drug-resistant strains. The ability to visualize bacteria *in vivo* can lead to advances in diagnosing infections and monitoring treatment. Taking advantage of maltodextrin transporters present in bacterial cells but not mammalian cells, Gambhir and co-workers functionalized a Cy7 derivative with maltotriose or maltohexose to facilitate dye uptake into bacteria (Figure 10a).³⁹ Initial competition experiments were performed to elucidate the mode of uptake using a radiotracer (^3H -maltose). After confirming this mechanism, an *E. coli*-induced myositis model was generated to evaluate performance *in vivo*. *E. coli* was injected intramuscularly to the left thigh and heat-inactivated *E. coli* was introduced to the right. PA imaging confirmed selective accumulation in the left *E. coli*-infected thigh. While a signal enhancement was observed with both maltotriose and maltohexose-labeled derivatives, the authors

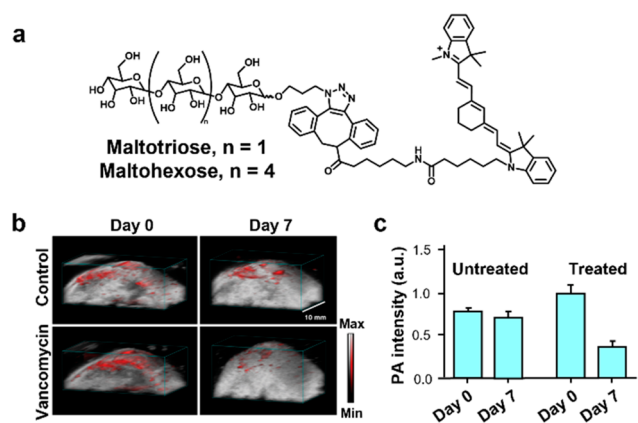


Figure 10. (a) Structure of Cy7-1-maltotriose and Cy7-1-maltohexose. (b) Representative PA images of a bacterial infection thigh model in mice before and after vancomycin treatment or saline treatment. (c) Quantified PA signal. Adapted with permission under a CC BY 4.0 license from ref 39. Copyright 2020 Springer Nature.

observed no significant difference between uptake between maltotriose and maltohexose-labeled derivatives. Furthermore, since *Staphylococcus aureus* infections are common in hospital settings, an *S. aureus* infection mouse model was also generated by subcutaneous inoculation into the back using a bioluminescent Xen 36 strain. One group received vancomycin treatment twice daily, and the other group received no antibiotics. After a week of treatment, bioluminescence and PA imaging both confirmed the decrease in signal from the bacterial infection (Figure 10b,c).

In another study, gold nanoparticles were developed to detect bacterial infection. Specifically, Zou, Li, Wang, and co-workers reported AuNP@P1, a P1 peptide surface labeled-gold nanoparticle.⁴⁰ The design of P1 includes three key elements: the assembly fragment (LVFFAED), enzyme-responsive linker (PLGVRG), and targeting ligand (RVRSA PSS). The latter enables accumulation of the nanoparticle in the bacterial microenvironment, where collagenase IV is overexpressed. Upon cleavage of the enzyme-responsive linker, the self-assembly fragment becomes exposed which allows for the nanoparticles to aggregate at the infection site through hydrogen bonding and π - π and hydrophobic interactions between the residues. This phenomenon increases the retention time via the aggregation/assembly induced retention effect and exhibits increased PA signal enhancement due to enhanced nanoparticle accumulation. A control nanoparticle, AuNP@P2, was also synthesized with a scrambled enzyme-responsive linker so that it would not aggregate in the presence of collagenase IV. Upon incubation with collagenase IV, AuNP@P1 exhibited an increase in absorbance at 710 nm due to aggregation while AuNP@P2 had no change. To examine its utility *in vivo*, *S. aureus* was injected into the hindlegs of mice. After 12 h, mice were treated with AuNP@P1 or AuNP@P2. PA imaging experiments concluded that accumulation had peaked 24 h postinjection with a 2-fold signal difference between the probe and control.

6.2. Virus Detection

Viral replication can lead to the expression of unique proteases that can be leveraged to detect viral infections. Jokerst and co-workers took advantage of the propensity for the cyanine dye platform to aggregate to develop a generalizable ABS probe for proteases (Figure 11a).⁴¹ J-Aggregation or H-aggregation was

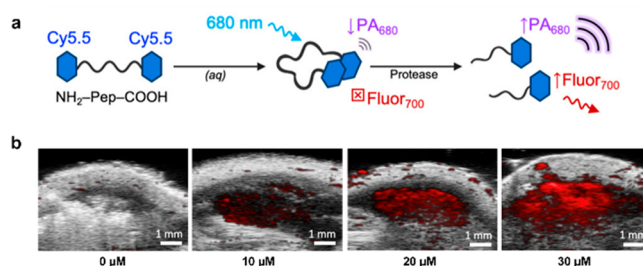


Figure 11. (a) Design principle of linking dyes to promote aggregation. (b) Representative PA images of mice injected with vehicle and trypsin-activated probe. Adapted from ref 41. Copyright 2021 American Chemical Society.

promoted by appending two molecules of a cyanine together through a peptide linker, leading to a shift in the maximum absorbance. Upon protease cleavage of the unique peptide sequence, the probe separates into two equivalents of monomeric cyanine. Since the PA signal is directly correlated to the number of photons absorbed, exciting at the maximum absorbance of the monomer (rather than the aggregates) allows for PA imaging of the turned over monomer. An initial proof-of-concept study was performed with a sequence recognized by trypsin *in vitro* to show a PA signal enhancement in the presence of this biomarker. Further, to show generalizability, the peptide sequence AVLQSGFR, recognized by M^{pro} from SARS-CoV-2, was inserted between two monomers. Upon introduction of M^{pro}, an increase in the PA signal was observed, motivating the use of this simple assay for the development of inhibitors for M^{pro}. Finally, the authors tested the probe *in vivo* by injecting nude mice with the probe that had been preactivated by trypsin prior to PA imaging (Figure 11b).

7. BLOOD CLOT IMAGING

7.1. Thrombosis Monitoring

Thrombin is an important enzyme involved in blood coagulation to close wounds. However, thrombosis occurs when a clot obstructs blood flow with potentially lethal consequences. On the other hand, if thrombosis can be located and resolved early using biomarkers such as thrombin and heparin, treatment can be lifesaving.⁴² Using thrombin as a biomarker for thrombosis, Lu, Chan, and co-workers developed the first activatable aptamer-based PA probe (Figure 12a).⁴³ The design principle relies on a fluorophore (IRDye 800CW) and a quencher (IRDye QC-1) pair which are each bound to a separate DNA aptamer. Both aptamers are hybridized to third aptamer containing a thrombin binding sequence. In the absence of thrombin, the fluorophore is in close proximity to the quencher and thus, exhibits a small PA₇₈₀/PA₇₂₅ ratio. However, in the presence of thrombin, the reduction of contact quenching results in a large PA₇₈₀/PA₇₂₅ ratio. To determine its utility in biological systems, the probe was tested in human serum spiked with varying amounts of thrombin, revealing a LOD of 344 nM. Furthermore, the probe was applied to an *in vivo* thrombosis model where mice were injected with thrombin in the left flank and PBS in the right flank. PA imaging revealed a larger ratiometric turn-on response on the thrombin flank, demonstrating probe activation had taken place (Figure 12b,c).

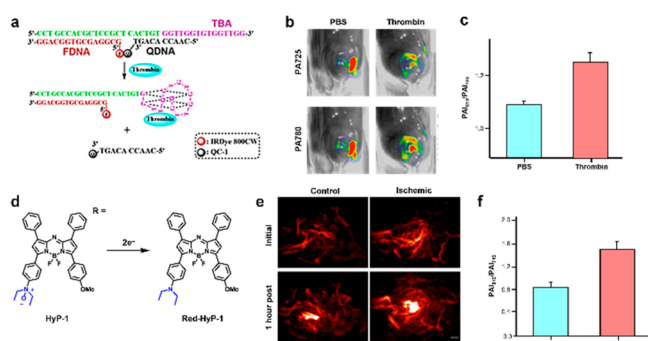


Figure 12. (a) Design principle of activatable DNA aptamers to detect thrombin in blood clotting. (b) Representative PA images at 725 and 780 nm. (c) PA fold turn-on between thrombin-treated mice and PBS-treated mice. Adapted from ref 43. Copyright 2017 American Chemical Society. (d) Structure of HyP-1 and its turnover product. (e) Representative PA images of an ischemia mouse model and nonischemia control. (f) Quantified PA fold turn-on. Adapted with permission under a CCBY 4.0 license from ref 44. Copyright 2017 Springer Nature.

7.2. Ischemic Hypoxia Sensing

Hypoxia is an important feature of peripheral artery diseases, liver injury, and gastrointestinal inflammation. It is defined as a situation where the demand for oxygen by tissue is greater than what is available. Notably, Chan and co-workers have developed HyP-1, a hypoxia-responsive PA probe based on the aza-BODIPY scaffold which features a *N*-oxide-based trigger (Figure 12d).⁴⁴ Under hypoxic conditions, CYP450 enzymes react with the *N*-oxide group, undergoing two-electron reduction to yield the uncapped dye (Red-HyP-1) which results in a red-shifted emission. HyP-1 has an absorbance and emission maxima at 670 and 697 nm, respectively, while red-HyP-1 (the turned over product) has

an absorbance and emission maxima at 760 and 798 nm, respectively. Due to the large Stokes shift, this platform was employed for multimodal (fluorescence and PA) ratiometric imaging. In their study, the authors generated a murine hindlimb ischemia model *via* ligation of the femoral artery to block blood flow. An hour after the procedure, mice were injected intramuscularly with HyP-1 and imaged using both modalities 1 h postinjection. Ratiometric fluorescence imaging exhibited a 3-fold increase in signal and PA imaging displayed a 3.1-fold turn-on response (Figure 12e,f). It is noteworthy that the *N*-oxide trigger developed in this study can detect acute hypoxia, whereas probes based on the traditional aryl nitro moiety can only detect chronic hypoxia due to the requirement for nitroreductase overexpression.

8. CONCLUSION

With the advent of activatable PA probes that employ an ABS design strategy, the detection and visualization of a wide range of biomarkers is now readily possible. Although the most common application of such probes is to study cancer-associated properties *in vivo*, the field has experienced tremendous growth in recent years to now include the molecular imaging of various other human disease states as we have highlighted in this review. A summary of the probes covered can be found in Table 1. The unique ability to reliably detect a molecular feature with high resolution and in deep tissue, sets PA imaging apart from other approaches. Indeed, this modality has already been used in humans to visualize inflammatory arthritis and scleroderma to name a few.^{45,46} However, it is notable that these representative clinical studies were performed in a label-free manner, and therefore, one would expect the ability to accurately diagnose these conditions will improve substantially when augmented with PA probes. In some instances, we anticipate that the application of PA probes can potentially replace invasive

Table 1. Summary of Small Molecule Probes Highlighted in This Review Article

name	λ_{abs}	biomarker	disease model	mode of activation	delivery method	Author(s); year
PA-HD-H ₂ O ₂ turnover	645 745	H ₂ O ₂	mouse Alzheimer's disease	uncapping	intravenous	Chan; 2021
RPS1	710	Cu ²⁺	mouse Alzheimer's disease	binding	intravenous	Sheng, Zhang; 2019
CaSPA	550	Ca ²⁺	zebrafish neurostimulation	binding	intraventricular	Westmeyer; 2018
PA-HD-MGL turnover	600 740	MGL	mouse inflammation	uncapping	intraperitoneal	Chan; 2022
PA-HD-FAAH turnover	658 730	FAAH	mouse inflammation	uncapping	intraperitoneal	Chan; 2022
APNO-5 turnover	764 673	NO	mouse inflammation	uncapping	subcutaneous	Chan; 2018
SR-APNO-3 turnover	790 690	NO	mouse flank tumor	uncapping	intratumoral	Chan; 2020
PACu-1 turnover	678 767	Cu ⁺	mouse Wilson's disease	uncapping	intraperitoneal	Chan; 2021
AP turnover	745 835	O ₂ ^{•-}	mouse liver injury	uncapping	intravenous	Ren, Yuan; 2022
DLP turnover	666 705	DLP	mouse liver injury	uncapping	intravenous	Zeng, Wu; 2019
HyP-1	670	hypoxia	mouse ischemic hypoxia	uncapping	intramuscular	Chan; 2017
Red-HyP-1	760					
octaphyrin	1200	pH	mouse stomach pH	N/A	intra-gastric	Sarma, Sessler, Liu; 2021
Cy7-1-maltotriose/hexose	750	maltodextrin transporter	mouse bacterial infections	N/A	intravenous	Gambhir; 2020
Cy5.5 dimers	680	protease activity	mouse viral infection	N/A	subcutaneous	Jokerst; 2021

biopsies such as for Wilson's disease (section 3.1). In order for PA probes to make a successful transition into the healthcare setting and become a mainstay, it is critical for probe markers to demonstrate utility in models beyond small laboratory animals. Indeed, the use of large animals (e.g., canine) exhibiting naturally occurring pathologies can expedite use in humans. Along these lines, probe developers should interface with bioengineers to actively develop PA imaging instrumentation for use in humans. On the probe development front, new PA-active dye platforms are highly desirable and should be actively pursued since the stronger the signal output, as predicted by a large PA brightness factor, can enable greater diagnostic accuracy.⁴⁷ Additionally, a move to the shortwave infrared window (section 4) can allow for greater tissue penetration as interference from endogenous absorbers like blood is minimized.

AUTHOR INFORMATION

Corresponding Author

Jefferson Chan – Department of Chemistry, Beckman Institute for Advanced Science and Technology, and Cancer Center at Illinois, University of Illinois at Urbana—Champaign, Urbana, Illinois 61801, United States;  orcid.org/0000-0003-4139-4379; Email: jeffchan@illinois.edu

Authors

Michael C. Lee – Department of Chemistry, Beckman Institute for Advanced Science and Technology, and Cancer Center at Illinois, University of Illinois at Urbana—Champaign, Urbana, Illinois 61801, United States;  orcid.org/0000-0001-8125-7120

Kayla Landers – Department of Chemistry, Beckman Institute for Advanced Science and Technology, and Cancer Center at Illinois, University of Illinois at Urbana—Champaign, Urbana, Illinois 61801, United States

Complete contact information is available at:
<https://pubs.acs.org/10.1021/acsbiomedchemau.3c00009>

Notes

The authors declare no competing financial interest.

ACKNOWLEDGMENTS

K.L. thanks the Summer Predoctoral Institute (SPI), California Predoctoral Program, NIH Chemistry-Biology Interface Training Grant (T32-GM136629). J.C. acknowledges the Camille and Henry Dreyfus Foundation for support. The authors thank the National Science Foundation (1752879) and the National Institutes of Health (R35GM133581) for supporting this work. The authors thank Mr. Oliver D Pichardo Peguero for drafting an early version of sections 5.1 and 5.2.

ABBREVIATIONS

TPA, tris[(2-pyridyl)methyl]amine; GSH, glutathione; PEG, polyethylene glycol; DPSE-PEG₂₀₀₀, distearoyl-*sn*-glycero-3-phosphoethanolamine-poly(ethylene glycol); LOD, limit of detection; NP, nanoparticle

REFERENCES

(1) Tsang, V. T. C.; Li, X.; Wong, T. T. W. A Review of Endogenous and Exogenous Contrast Agents Used in Photoacoustic Tomography with Different Sensing Configurations. *Sensors (Switzerland)* **2020**, *20* (19), 5598.

(2) Li, M.; Tang, Y.; Yao, J. Photoacoustic Tomography of Blood Oxygenation: A Mini Review. *Photoacoustics* **2018**, *10*, 65–73.

(3) Levi, J.; Kothapalli, S. R.; Bohndiek, S.; Yoon, J. K.; Dragulescu-Andrasi, A.; Nielsen, C.; Tisma, A.; Bodapati, S.; Gowrishankar, G.; Yan, X.; Chan, C.; Starcevic, D.; Gambhir, S. S. Molecular Photoacoustic Imaging of Follicular Thyroid Carcinoma. *Clin. Cancer Res.* **2013**, *19* (6), 1494–1502.

(4) Gardner, S. H.; Reinhardt, C. J.; Chan, J. Advances in Activity-Based Sensing Probes for Isoform-Selective Imaging of Enzymatic Activity. *Angew. Chemie - Int. Ed.* **2021**, *60* (10), 5000–5009.

(5) East, A. K.; Lucero, M. Y.; Chan, J. New Directions of Activity-Based Sensing for in Vivo NIR Imaging. *Chem. Sci.* **2021**, *12* (10), 3393–3405.

(6) Chan, J.; Dodani, S. C.; Chang, C. J. Reaction-Based Small-Molecule Fluorescent Probes for Chemoselective Bioimaging. *Nat. Chem.* **2012**, *4* (12), 973–984.

(7) Bruemmer, K. J.; Crossley, S. W. M.; Chang, C. J. Activity-Based Sensing: A Synthetic Methods Approach for Selective Molecular Imaging and Beyond. *Angew. Chemie - Int. Ed.* **2020**, *59* (33), 13734–13762.

(8) Yao, J.; Wang, L. V. Photoacoustic Brain Imaging: From Microscopic to Macroscopic Scales. *Neurophotonics* **2014**, *1* (1), 011003.

(9) Cash, K. J.; Li, C.; Xia, J.; Wang, L. V.; Clark, H. A. Optical Drug Monitoring: Photoacoustic Imaging of Nanosensors to Monitor Therapeutic Lithium in Vivo. *ACS Nano* **2015**, *9* (2), 1692–1698.

(10) Alzheimer's Association Report.. 2021 Alzheimer's disease facts and figures. *Alzheimer's & Dementia* **2021**, *17* (3), 327–406.

(11) Bloom, G. S. Amyloid- β and Tau: The Trigger and Bullet in Alzheimer Disease Pathogenesis. *JAMA Neurol.* **2014**, *71* (4), 505–508.

(12) Gardner, S. H.; Brady, C. J.; Keeton, C.; Yadav, A. K.; Mallojjala, S. C.; Lucero, M. Y.; Su, S.; Yu, Z.; Hirschi, J. S.; Mirica, L. M.; Chan, J. A General Approach to Convert Hemicyanine Dyes into Highly Optimized Photoacoustic Scaffolds for Analyte Sensing**. *Angew. Chem., Int. Ed.* **2021**, *60* (34), 18860–18866.

(13) Huang, W. J.; Zhang, X.; Chen, W. W. Role of Oxidative Stress in Alzheimer's Disease. *Biomed. Reports* **2016**, *4* (5), 519–522.

(14) Wang, S.; Sheng, Z.; Yang, Z.; Hu, D.; Long, X.; Feng, G.; Liu, Y.; Yuan, Z.; Zhang, J.; Zheng, H.; Zhang, X. Activatable Small-Molecule Photoacoustic Probes That Cross the Blood–Brain Barrier for Visualization of Copper(II) in Mice with Alzheimer's Disease. *Angew. Chem., Int. Ed.* **2019**, *58* (36), 12415–12419.

(15) Brini, M.; Cali, T.; Ottolini, D.; Carafoli, E. Neuronal Calcium Signaling: Function and Dysfunction. *Cell. Mol. Life Sci.* **2014**, *71* (15), 2787–2814.

(16) Russell, J. T. Imaging Calcium Signals in Vivo: A Powerful Tool in Physiology and Pharmacology. *Br. J. Pharmacol.* **2011**, *163* (8), 1605–1625.

(17) Roberts, S.; Seeger, M.; Jiang, Y.; Mishra, A.; Sigmund, F.; Stelzl, A.; Lauri, A.; Symvoulidis, P.; Rolbieski, H.; Preller, M.; Deán-Ben, X. L.; Razansky, D.; Orschmann, T.; Desbordes, S. C.; Vetschera, P.; Bach, T.; Ntziachristos, V.; Westmeyer, G. G. Calcium Sensor for Photoacoustic Imaging. *J. Am. Chem. Soc.* **2018**, *140* (8), 2718–2721.

(18) Kim, T.; Lemaster, J. E.; Chen, F.; Li, J.; Jokerst, J. V. Photoacoustic Imaging of Human Mesenchymal Stem Cells Labeled with Prussian Blue-Poly(L-Lysine) Nanocomplexes. *ACS Nano* **2017**, *11* (9), 9022–9032.

(19) Ludwig, J.; Moyer, T. P.; Rakela, J. The Liver Biopsy Diagnosis of Wilson's Disease: Methods in Pathology. *Am. J. Clin. Pathol.* **1994**, *102* (4), 443–446.

(20) Lucero, M. Y.; Tang, Y.; Zhang, C. J.; Su, S.; Forzano, J. A.; Garcia, V.; Huang, X.; Moreno, D.; Chan, J. Activity-Based Photoacoustic Probe for Biopsy-Free Assessment of Copper in Murine Models of Wilson's Disease and Liver Metastasis. *Proc. Natl. Acad. Sci. U. S. A.* **2021**, *118* (36), e2106943118.

(21) Wu, Y.; Huang, S.; Wang, J.; Sun, L.; Zeng, F.; Wu, S. Activatable Probes for Diagnosing and Positioning Liver Injury and

- Metastatic Tumors by Multispectral Photoacoustic Tomography. *Nat. Commun.* **2018**, *9* (1), 3983.
- (22) Ai, X.; Wang, Z.; Cheong, H.; Wang, Y.; Zhang, R.; Lin, J.; Zheng, Y.; Gao, M.; Xing, B. Multispectral Photoacoustic Imaging of Dynamic Redox Correlation and Pathophysiological Progression Utilizing Upconversion Nanoprobes. *Nat. Commun.* **2019**, *10* (1), 1–11.
- (23) Sun, L.; Wu, Y.; Chen, J.; Zhong, J.; Zeng, F.; Wu, S. A Turn-on Photoacoustic Probe for Imaging Metformin-Induced Upregulation of Hepatic Hydrogen Sulfide and Subsequent Liver Injury. *Theranostics* **2019**, *9* (1), 77–89.
- (24) Zhuang, H.; Li, B.; Zhao, M.; Wei, P.; Yuan, W.; Zhang, M.; Han, X.; Chen, Y.; Yi, T. Real-Time Monitoring and Accurate Diagnosis of Drug-Induced Hepatotoxicity in Vivo by Ratio-Fluorescence and Photoacoustic Imaging of Peroxynitrite. *Nanoscale* **2020**, *12* (18), 10216–10225.
- (25) Fan, X.; Ren, T.; Yang, W.; Zhang, X.; Yuan, L. Activatable Photoacoustic/Fluorescent Dual-Modal Probe for Monitoring of Drug-Induced Liver Hypoxia: In Vivo. *Chem. Commun.* **2021**, 57 (69), 8644–8647.
- (26) Roberts, S.; Khera, E.; Choi, C.; Navaratna, T.; Grimm, J.; Thurber, G. M.; Reiner, T. Photoacoustic Imaging of Glucagon-like Peptide-1 Receptor with a near-Infrared Exendin-4 Analog. *J. Nucl. Med.* **2021**, *62* (6), 839–848.
- (27) East, A. K.; Lee, M. C.; Smaga, L. P.; Jiang, C.; Mallojjala, S. C.; Hirschi, J. S.; Chan, J. Synthesis of Silicon-Substituted Hemicyanines for Multimodal SWIR Imaging. *Org. Lett.* **2022**, *24*, 8509.
- (28) Qiu, Z.; Zhang, C.; Zhang, L.; Wang, S.; Hu, S.; Zhao, S. Precise in Vivo Inflammation Imaging in the NIR-II Window Using 1065 Nm Photoacoustic Probe for in Situ Visual Monitoring of Pathological Processes Related to Hepatitis. *ACS Sensors* **2022**, *7* (2), 641–648.
- (29) Wu, H.; Xia, F.; Zhang, L.; Fang, C.; Lee, J.; Gong, L.; Gao, J.; Ling, D.; Li, F. A ROS-Sensitive Nanozyme-Augmented Photoacoustic Nanoprobe for Early Diagnosis and Therapy of Acute Liver Failure. *Adv. Mater.* **2022**, *34* (7), e2108348.
- (30) Fan, X. P.; Yang, W.; Ren, T. B.; Xu, S.; Gong, X. Y.; Zhang, X. B.; Yuan, L. Engineering a Ratiometric Photoacoustic Probe with a Hepatocyte-Specific Targeting Ability for Liver Injury Imaging. *Anal. Chem.* **2022**, *94* (2), 1474–1481.
- (31) Huang, Y.; Qi, Y.; Zhan, C.; Zeng, F.; Wu, S. Diagnosing Drug-Induced Liver Injury by Multispectral Photoacoustic Tomography and Fluorescence Imaging Using a Leucine-Aminopeptidase-Activated Probe. *Anal. Chem.* **2019**, *91* (13), 8085–8092.
- (32) Chen, J.; Sedgwick, A. C.; Sen, S.; Ren, Y.; Sun, Q.; Chau, C.; Arambula, J. F.; Sarma, T.; Song, L.; Sessler, J. L.; Liu, C. Expanded Porphyrins: Functional Photoacoustic Imaging Agents That Operate in the NIR-II Region. *Chem. Sci.* **2021**, *12* (29), 9916–9921.
- (33) Van Egmond, N.; Straub, V. M.; Van Der Stelt, M. Targeting Endocannabinoid Signaling: FAAH and MAG Lipase Inhibitors. *Annu. Rev. Pharmacol. Toxicol.* **2021**, *61*, 441–463.
- (34) Lucero, M. Y.; Gardner, S. H.; Yadav, A. K.; Borri, A.; Zhao, Z.; Chan, J. Activity-Based Photoacoustic Probes Reveal Elevated Intestinal MGL and FAAH Activity in a Murine Model of Obesity. *Angew. Chem., Int. Ed.* **2022**, *61* (44), e202211774.
- (35) Chen, K.; Pittman, R. N.; Popel, A. S. Nitric Oxide in the Vasculature: Where Does It Come from and Where Does It Go? A Quantitative Perspective. *Antioxidants Redox Signal.* **2008**, *10* (7), 1185–1198.
- (36) Reinhardt, C. J.; Zhou, E. Y.; Jorgensen, M. D.; Partipilo, G.; Chan, J. A Ratiometric Acoustogenic Probe for in Vivo Imaging of Endogenous Nitric Oxide. *J. Am. Chem. Soc.* **2018**, *140* (3), 1011–1018.
- (37) Reinhardt, C. J.; Xu, R.; Chan, J. Nitric Oxide Imaging in Cancer Enabled by Steric Relaxation of a Photoacoustic Probe Platform. *Chem. Sci.* **2020**, *11* (6), 1587–1592.
- (38) Chen, L.; Ji, Y.; Hu, X.; Cui, C.; Liu, H.; Tang, Y.; Qi, B.; Niu, Y.; Hu, X.; Yu, A.; Fan, Q. Cationic Poly-l-Lysine-Encapsulated Melanin Nanoparticles as Efficient Photoacoustic Agents Targeting Glycosaminoglycans for the Early Diagnosis of Articular Cartilage Degeneration in Osteoarthritis. *Nanoscale* **2018**, *10* (28), 13471–13484.
- (39) Zlitni, A.; Gowrishankar, G.; Steinberg, I.; Haywood, T.; Sam Gambhir, S. Maltotriose-Based Probes for Fluorescence and Photoacoustic Imaging of Bacterial Infections. *Nat. Commun.* **2020**, *11* (1), 1–13.
- (40) Lu, S. Z.; Guo, X. Y.; Zou, M. S.; Zheng, Z. Q.; Li, Y. C.; Li, X. D.; Li, L. L.; Wang, H. Bacteria-Instructed In Situ Aggregation of AuNPs with Enhanced Photoacoustic Signal for Bacterial Infection Bioimaging. *Adv. Healthc. Mater.* **2020**, *9* (1), 1901229.
- (41) Moore, C.; Borum, R. M.; Mantri, Y.; Xu, M.; Fajtová, P.; O'Donoghue, A. J.; Jokerst, J. V. Activatable Carbocyanine Dimers for Photoacoustic and Fluorescent Detection of Protease Activity. *ACS Sensors* **2021**, *6* (6), 2356–2365.
- (42) Yim, W.; Takemura, K.; Zhou, J.; Zhou, J.; Jin, Z.; Borum, R. M.; Xu, M.; Cheng, Y.; He, T.; Penny, W.; Miller, B. R.; Jokerst, J. V. Enhanced Photoacoustic Detection of Heparin in Whole Blood via Melanin Nanocapsules Carrying Molecular Agents. *ACS Nano* **2022**, *16* (1), 683–693.
- (43) Zhang, J.; Smaga, L. P.; Satyavolu, N. S. R.; Chan, J.; Lu, Y. DNA Aptamer-Based Activatable Probes for Photoacoustic Imaging in Living Mice. *J. Am. Chem. Soc.* **2017**, *139* (48), 17225–17228.
- (44) Knox, H. J.; Hedhli, J.; Kim, T. W.; Khalili, K.; Dobrucki, L. W.; Chan, J. A Bioreducible N-Oxide-Based Probe for Photoacoustic Imaging of Hypoxia. *Nat. Commun.* **2017**, *8* (1), 1794.
- (45) Jo, J.; Xu, G.; Cao, M.; Marquardt, A.; Francis, S.; Gandikota, G.; Wang, X. A Functional Study of Human Inflammatory Arthritis Using Photoacoustic Imaging. *Sci. Rep.* **2017**, *7* (1), 1–9.
- (46) Liu, Y.; Zhang, L.; Li, S.; Han, X.; Yuan, Z. Imaging Molecular Signatures for Clinical Detection of Scleroderma in the Hand by Multispectral Photoacoustic Elastic Tomography. *J. Biophotonics* **2018**, *11* (6), e201700267.
- (47) Zhou, E. Y.; Knox, H. J.; Liu, C.; Zhao, W.; Chan, J. A Conformationally Restricted Aza-BODIPY Platform for Stimulus-Responsive Probes with Enhanced Photoacoustic Properties. *J. Am. Chem. Soc.* **2019**, *141* (44), 17601–17609.